

1 *Supplement of*

2 **Large contribution of soil emissions to the atmospheric nitrogen**  
3 **budget and their impacts on air quality and temperature rise in**  
4 **North China**

5 *Tong Sha<sup>1\*</sup>, Siyu Yang<sup>1</sup>, Qingcai Chen<sup>1</sup>, Liangqing Li<sup>1</sup>, Xiaoyan Ma<sup>2</sup>, Yan-Lin Zhang<sup>3,4</sup>,*

6 *Zhaozhong Feng<sup>3</sup>, K. Folkert Boersma<sup>5,6</sup>, Jun Wang<sup>7\*</sup>*

7 <sup>1</sup> School of Environmental Science and Engineering, Shaanxi University of Science and  
8 Technology, Xi'an 710021, China

9 <sup>2</sup> Key Laboratory for Aerosol-Cloud-Precipitation of China Meteorological  
10 Administration, Nanjing University of Information Science & Technology, Nanjing  
11 210044, China

12 <sup>3</sup> School of Ecology and Applied Meteorology, Nanjing University of Information  
13 Science & Technology, Nanjing 210044, China

14 <sup>4</sup> Atmospheric Environment Center, Joint Laboratory for International Cooperation on  
15 Climate and Environmental Change, Ministry of Education (ILCEC), Nanjing  
16 University of Information Science & Technology, Nanjing 210044, China

17 <sup>5</sup> Satellite Observations Department, Royal Netherlands Meteorological Institute, De  
18 Bilt 3731GA, the Netherlands

19 <sup>6</sup> Meteorology and Air Quality Group, Wageningen University Wageningen 6708PB,  
20 the Netherlands

21 <sup>7</sup> Department of Chemical and Biochemical Engineering, Center for Global and  
22 Regional Environmental Research, and Iowa Technology Institute, University of Iowa,  
23 Iowa City, IA, 52242, USA

24 \*Corresponding authors:

25 Tong Sha: [tong-sha@sust.edu.cn](mailto:tong-sha@sust.edu.cn)

26 Jun Wang, [jun-wang-1@uiowa.edu](mailto:jun-wang-1@uiowa.edu)

27

28 **Text S1. Parameterization of HONO sources**

29 In the present study, we incorporated five additional HONO sources in the WRF-  
30 Chem model, as described below.

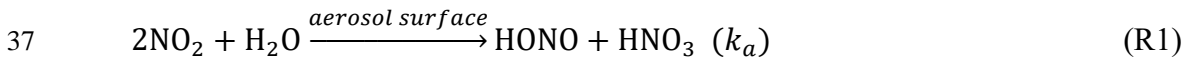
31 1. Direct traffic emissions

32 The traffic emission was calculated by a HONO/NO<sub>x</sub> ratio of 1.7% (Rappenglück  
33 et al., 2013), which is the same as the setting of (Zhang et al., 2019).

34 2. The HONO source from soil emissions

35 See section 2.1.2 in the manuscript.

36 3. Heterogeneous source on aerosol surface



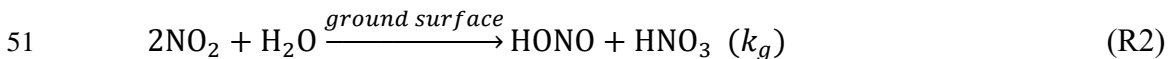
38 Most studies suggested that the heterogeneous reaction of NO<sub>2</sub> to HONO was first  
39 order in NO<sub>2</sub> (Finlayson-Pitts et al., 2003; Saliba et al., 2000), thus for the NO<sub>2</sub>  
40 heterogeneous reaction on the aerosol surface, the first-order reaction rate constant  $k_a$   
41 is estimated by (Li et al., 2010) and (Zhang et al., 2016) as follows:

42 
$$k_a = \frac{1}{4} \cdot v_{\text{NO}_2} \cdot \left(\frac{S_a}{V}\right) \cdot \gamma_{\text{a-NO}_2} \quad (1)$$

43 where  $v_{\text{NO}_2}$  is the mean molecular velocity of NO<sub>2</sub> (m s<sup>-1</sup>),  $S_a/V$  is the aerosol surface  
44 to volume ratio (m<sup>-1</sup>) representing the surface available for heterogeneous reaction.  
45  $\gamma_{\text{a-NO}_2}$  is the uptake coefficient of NO<sub>2</sub> at the aerosol surface, which was set to be  $1 \times$   
46  $10^{-6}$  for nighttime, and a higher value of  $2 \times 10^{-5}$  applied for daytime when the light  
47 intensity (LI) was lower than 400 W m<sup>-2</sup>, whereas we linearly scaled it with solar  
48 radiation when the light intensity was higher than 400 W m<sup>-2</sup> (equation 2).

49 
$$\gamma_{\text{a-NO}_2} = \begin{cases} 1 \times 10^{-6} \text{ (nighttime)} \\ 2 \times 10^{-5} \cdot \left(\frac{\text{LI}}{400}\right) \text{ (daytime, LI} \geq 400 \text{ W m}^{-2}\text{)} \\ 2 \times 10^{-5} \text{ (daytime, LI} < 400 \text{ W m}^{-2}\text{)} \end{cases} \quad (2)$$

50 4. Heterogeneous source on ground surface



52 For the NO<sub>2</sub> heterogeneous reaction on ground surface (R2), the first-order  
53 reaction rate constant  $k_g$  is estimated by (Zhang et al., 2016) as follows:

54 
$$k_g = \frac{1}{8} \cdot v_{\text{NO}_2} \cdot \left(\frac{S_g}{V}\right) \cdot \gamma_{\text{g-NO}_2} \quad (3)$$

55 where  $v_{\text{NO}_2}$  is the mean molecular velocity of  $\text{NO}_2$  ( $\text{m s}^{-1}$ ),  $S_g/V$  represents the ground  
56 surface to volume ratio. Over the urban areas as defined by the MODIS land use data,  
57 we adopted a constant  $S_g/V$  value of  $0.3 \text{ m}^{-1}$ . For the vegetation-covered areas, the leaf  
58 area index (LAI,  $\text{m}^2/\text{m}^2$ ) and the height of the first model layer ( $H$ , m) were used to  
59 estimate the surface area to volume ratio following the method in (Sarwar et al., 2008):

$$60 \quad \frac{S_g}{V} = \frac{2 \times \text{LAI}}{H} \quad (4)$$

61  $\gamma_{\text{g-NO}_2}$  is the uptake coefficient of  $\text{NO}_2$  at the ground surface and is assumed to be the  
62 same as that for aerosol surface. The heterogeneous reaction of  $\text{NO}_2$  on the ground  
63 surface was only considered within the first model layer, whereas that on the aerosol  
64 surface was treated in all model layers.

#### 65 5. Inorganic nitrate photolysis

66 The photolysis reaction of particulate nitrate in the atmosphere to produce HONO  
67 and  $\text{NO}_2$  (R3) was added in the WRF-Chem model following the work of (Fu et al.,  
68 2019).



70 The photolysis rate of particulate nitrate was estimated by a  $J_{\text{nitrate}}/J_{\text{HNO}_3}$  ratio of  
71  $\frac{8.3 \times 10^{-5}}{7 \times 10^{-7}}$ , where  $J_{\text{HNO}_3}$  is the photolysis rate of gaseous  $\text{HNO}_3$  simulated online in the  
72 model.

73

74 **Table S1** Total annual N fertilizer application from 2006 to 2018 (unit: 10 Gg N yr<sup>-1</sup>),  
 75 and the adjustment coefficient (2006 vs. 2018, unit: %) for N fertilizer application in  
 76 each province.

Province	2006	2007	2008	2009	2010	2011	2012	2013	2014	2015	2016	2017	2018	2006vs.2018
<b>Neimenggu</b>	64	68	73	80	80	81	83	89	97	99	98	95	86	34.5
<b>Gansu</b>	37	38	38	38	38	38	40	40	41	41	39	34	33	-9.6
<b>Ningxia</b>	16	17	17	17	18	18	18	19	18	17	17	17	16	4.5
<b>Shaanxi</b>	76	81	81	87	88	91	98	99	96	94	92	90	89	16.2
<b>Shanxi</b>	41	41	40	39	40	39	39	38	36	34	32	28	25	-38
<b>Hebei</b>	155	156	153	153	153	152	152	151	151	148	145	140	114	-26.2
<b>Beijing</b>	8	7	7	7	7	7	6	6	5	5	4	4	3	-61.3
<b>Tianjin</b>	12	13	12	12	12	11	11	11	11	10	9	7	6	-53.6
<b>Henan</b>	235	239	240	239	244	245	246	244	241	239	228	220	202	-14.3
<b>Shandong</b>	194	193	170	165	163	159	160	158	154	151	146	139	131	-32.5
<b>Jiangsu</b>	183	183	181	182	180	174	169	166	164	162	158	151	146	-20.4
<b>Anhui</b>	112	111	112	112	112	114	114	114	112	108	105	101	96	-14.4
<b>Huibe</b>	140	143	149	154	156	159	159	153	146	139	134	128	113	-19.5
<b>Chongqing</b>	46	48	50	50	49	50	50	50	50	50	48	47	46	-1.1
<b>Sichuan</b>	125	128	129	131	130	129	128	126	126	125	122	117	112	-10.1
<b>Liaoning</b>	63	65	66	67	68	70	68	70	68	66	60	57	55	-13.5

78 **Table S2.** Soil categories used in (Oswald et al., 2013).

<b>No.</b>	<b>Soil Category in Oswald et al. (2013)</b>
<b>S1</b>	eucalyptus forest, Grose Valley, Australia
<b>S2</b>	tropical rain forest, Suriname
<b>S3</b>	coniferous forest, Hohenpeißenberg, Germany
<b>S4</b>	coniferous forest, Fichtelgebirge, Germany
<b>S5</b>	pasture, Hawkesbury River flood plain, Australia
<b>S6</b>	open woody savannah, Dahra, Senegal
<b>S7</b>	open woody savannah, Agoufou, Mali
<b>S8</b>	grassland, Mainz-Finthen, Germany
<b>S9</b>	pasture, Hohenpeißenberg, Germany
<b>S10</b>	stone desert, Ruta B 376, Chile
<b>S11</b>	maize field, Grignon, France
<b>S12</b>	wheat field, Mainz-Finthen, Germany
<b>S13</b>	jujube field, Qiemo, China
<b>S14</b>	cotton field, Qiemo, China
<b>S15</b>	jujube field, Mingfeng, China
<b>S16</b>	stone desert, Sache, China
<b>S17</b>	cotton field, Milan, China

79

80 **Table S3.** Emission factor of 20 soil biomes based on MODIS land cover types.

<b>ID</b>	<b>MODIS land cover type</b>	<b>MEDIUM</b>	<b>HIGH</b>	<b>LOW</b>
1	Evergreen needleleaf forest	S3, S4	S3	S4
2	Evergreen broadleaf forest	S2	S2	S2
3	Deciduous needleleaf forest	S3, S4	S3	S4
4	Deciduous broadleaf forest	S1	S1	S1
5	Mixed forest	S1, S2, S3, S4	S2	S4
6	Closed shrublands	S6, S7, S8	S6	S8
7	Open shrublands	S6, S7	S6	S7
8	Woody savannas	--	--	--
9	Savannas	S6, S7	S6	S7
10	Grasslands	S8	S8	S8
11	Permanent wetlands	--	--	--
12	Croplands	S5, S9, S11, S12, S14, S17	S12	S9
13	Urban and built-up	--	--	--
14	Cropland/Natural vegetation mosaic	S8, S5, S9, S11, S12, S14, S17	S12	S9
15	Snow and ice	--	--	--
16	Barren or sparsely vegetated	S16, S10	S10	S16
17	water	--	--	--
18	Wooded tundra	--	--	--
19	Mixed tundra	--	--	--
20	Barren Tundra	--	--	--

81

82 **Table S4.** The optimum SHONO fluxes used in this study and other literature.

ID	MODIS land cover type	Optimum SHONO fluxes ( $\text{ng m}^{-2} \text{s}^{-1}$ )	References (land cover type in local scale)
1	Evergreen needleleaf forest	<b>0.549</b>	this study
2	Evergreen broadleaf forest	<b>2.872</b>	this study
3	Deciduous needleleaf forest	<b>0.549</b>	this study
4	Deciduous broadleaf forest	<b>0.887</b>	this study
		<b>1.214</b>	this study
		1.3	Zhou et al. (2011)
5	Mixed forest	0.01-104.72 (mean=16.45)	Wu et al. (2022)
		0.2-208 (mean=50)	Wang et al. (2023)
6	Closed shrublands	<b>20.57</b>	this study
7	Open shrublands	<b>29.779</b>	this study
8	Woody savannas	--	--
		<b>9.926</b>	this study
9	Savannas	1.1	Weber B (2015)
		<b>2.154</b>	this study
10	Grasslands	1.0	Twigg et al. (2011)
		0.1-74.27(mean =17.57)	Wu et al. (2022)
11	Permanent wetlands	--	--
		<b>30.036</b>	this study
		1.42-376.01(mean =119.8)	Wu et al. (2019, 2022)
		0.84±2.38	Meng et al. (2022)
12	Croplands	-1.32-7.69 (mean=2.94)	Tang et al. (2020)
		3.21	Xue et al. (2019)
		16-484	Wang et al. (2023)
13	Urban and built-up	--	--
14	Cropland/Natural vegetation mosaic	<b>25.847</b>	this study
15	Snow and ice	--	--
16	Barren or sparsely vegetated	<b>14.742</b>	this study

		1.5	Weber B (2015)
		5.38-288.23 (mean=57.06)	Wu et al. (2022)
<b>17</b>	water	--	--
<b>18</b>	Wooded tundra	--	--
<b>19</b>	Mixed tundra	--	--
<b>20</b>	Barren Tundra	--	--

---

83



84 **Table S5.** Description of model simulation experiments.

Simulation	Soil emissions		Anthropogenic emissions
	Soil NO <sub>x</sub>	Soil HONO	NO <sub>x</sub>
<b>Default</b>	1(MEGAN)	0	1
<b>Base</b>	1(BDISNP)	1	1
<b>NoSoilNr</b>	0	0	1
<b>NoSHONO</b>	1	0	1
<b>NoSNO<sub>x</sub></b>	0	1	1
<b>Base_redANO<sub>x</sub></b>	1	1	0.8/0.6/0.4/0.2/0 <sup>a</sup>
<b>NoSoil_redANO<sub>x</sub></b>	0	0	0.8/0.6/0.4/0.2/0 <sup>b</sup>

85 <sup>a, b</sup> The values represent the reduction ratios applied to the anthropogenic NO<sub>x</sub> emissions in the  
 86 sensitivity simulations compared to the Base.

87

88 **Table S6.** Contribution of soil NO<sub>x</sub> and HONO emissions to monthly average surface  
 89 concentrations of NO<sub>2</sub> and HONO (unit: %).

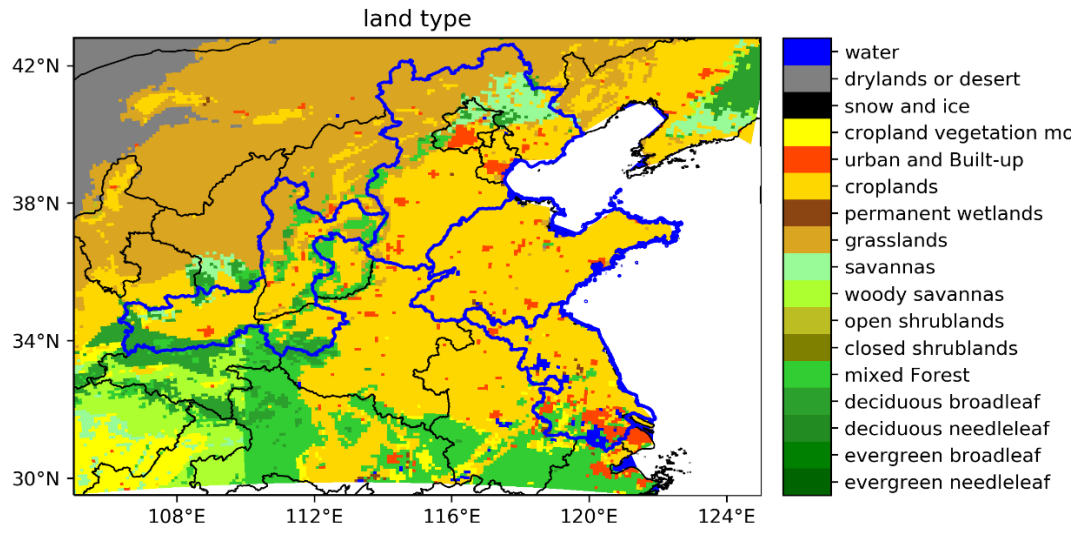
Contribution	Surface NO <sub>2</sub> concentrations			Surface HONO concentrations		
	Study region (CL)	BTH(CL)	FWP(CL)	Study region (CL)	BTH(CL)	FWP(CL)
SNO <sub>x</sub>	30.3(33.2)	37.1(39.5)	31.8(38.6)	6.2(5.7)	7.8(7.6)	4.95(4.2)
SHONO	3.1(2.3)	1.8(1.75)	2.7(3.1)	35.6 (38.7)	36.7(38.6)	38.0(42.7)
Soil Nr	32.7(34.7)	38.4(40.5)	33.9(41.3)	38.2(20.0)	40.3(42.0)	40.1(44.6)

90

91 **Table S7.** Effect of soil NO<sub>x</sub> and HONO emissions on monthly average surface  
 92 concentrations of MDA8 O<sub>3</sub>, max-1h OH, and nitrate in BTH and FWP region during  
 93 July 2018 (unit: %).

Change	MDA8 O <sub>3</sub>			max-1h ·OH			nitrate		
	Study region (CL)	BTH (CL)	FWP (CL)	Study region (CL)	BTH (CL)	FWP (CL)	Study region (CL)	BTH (CL)	FWP (CL)
Soil NO <sub>x</sub>	15.3 (17.4)	13.9 (15.0)	14.6 (15.6)	-31.3 (-21.6)	-28.4 (-13.5)	-38.6 (-24.8)	17.8 (22.4)	29.6 (41.3)	27.6 (32.8)
Soil HONO	3.3 (3.0)	3.5 (3.8)	2.8 (3.1)	10.0 (13.4)	9.3 (13.1)	10.3 (17.5)	10.4 (11.3)	10.9 (14.2)	13.5 (15.2)
Soil Nr	18.2 (20.0)	16.9 (18.1)	17.2 (18.6)	-24.3 (-12.5)	-22.6 (-4.4)	-32.2 (-13.6)	31.8 (35.8)	42.4 (57.8)	42.7 (49.9)

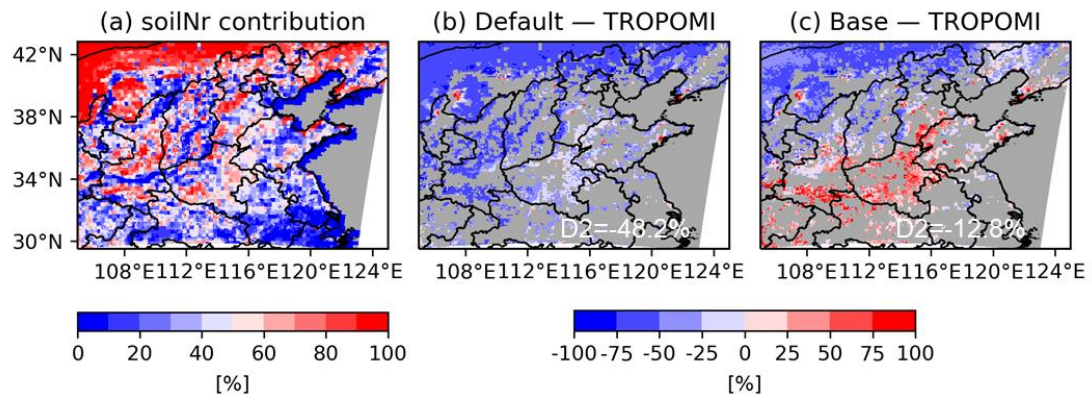
94



95

96 **Figure S1.** The land cover type over the simulation domain.

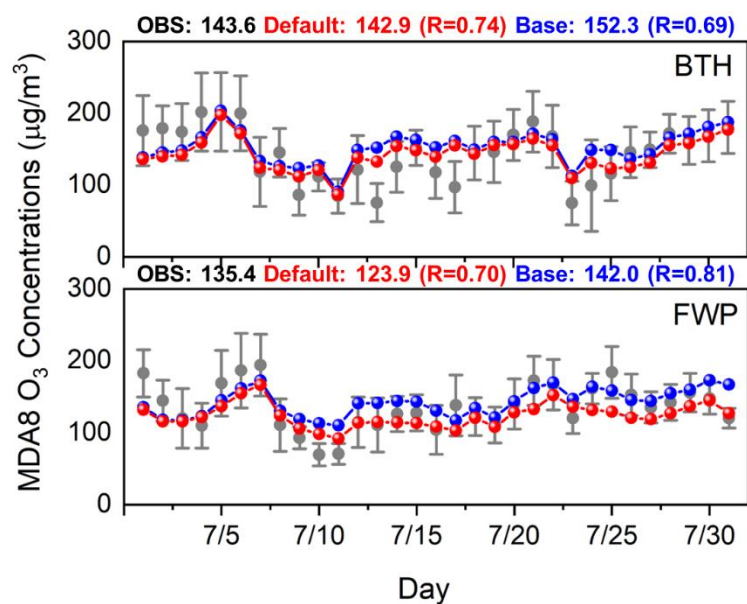
97



99

100 **Figure S2.** (a) Distribution of simulated contribution of soil Nr emissions to total Nr  
 101 emissions, which includes the sources from anthropogenic emissions, soil emissions,  
 102 and biomass burning. The difference of monthly mean tropospheric NO<sub>2</sub> VCD from  
 103 TROPOMI observations and simulations ((b) Default, (c) Base). Statistics in each panel  
 104 are the mean value averaged over the study region.

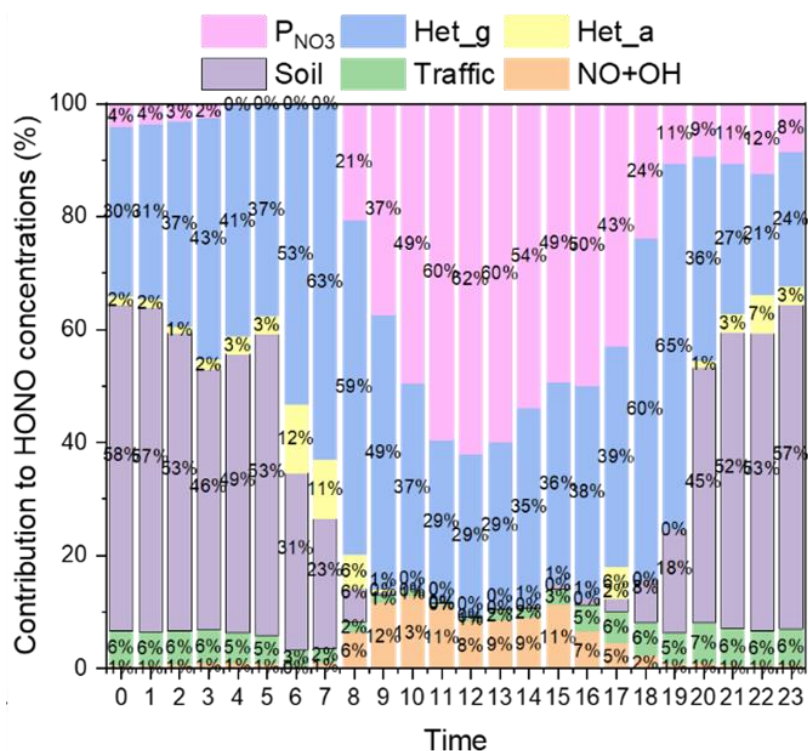
105



106

107 **Figure S3.** Time series of observed (grey circles with bars representing the standard  
 108 deviations) and simulated (Default in red and Base in blue) surface MDA8 O<sub>3</sub>  
 109 concentrations in the BTH and FWP regions, with the mean value and temporal  
 110 correlation coefficients (R) shown in the upper corner.

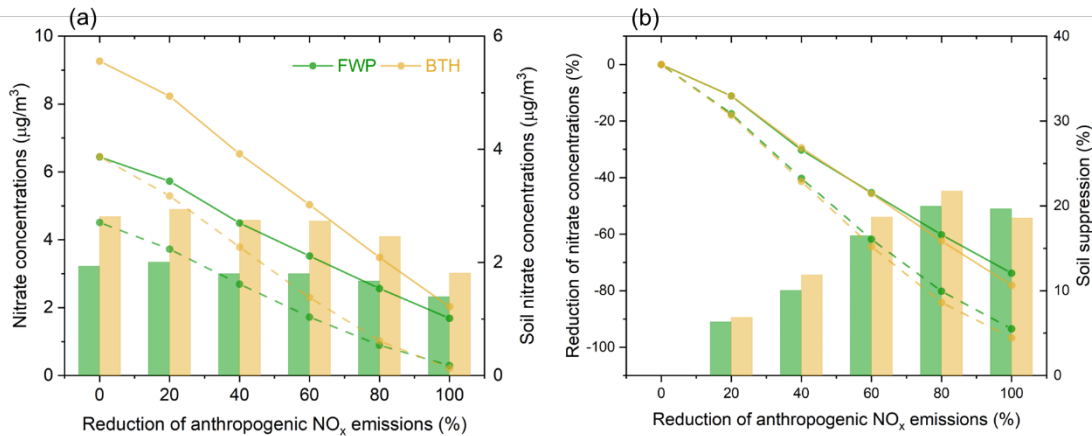
111



112

113 **Figure S4.** Average diurnal variations of contributions of different HONO sources to  
 114 the simulated surface HONO at a rural station in Nanjing during July 2018. (P<sub>NO3</sub>,  
 115 Het<sub>g</sub>, Het<sub>a</sub>, Soil, Traffic, and NO+OH represent HONO sources from the inorganic  
 116 nitrate photolysis in the atmosphere, NO<sub>2</sub> heterogeneous reactions on ground and  
 117 aerosol surfaces, soil emissions, traffic emissions, and the gas-phase formation,  
 118 respectively).

119



121

122 **Figure S5.** The responses of nitrate concentrations to the reductions of anthropogenic  
 123 NO<sub>x</sub> emissions (20%, 40%, 60%, 80% and 100%) relative to July 2018 levels in the  
 124 presence (solid line) and absence (dotted line) of soil nitrogen emissions. (The lines in  
 125 panel (a-b) are the nitrate concentrations and the relative reductions in nitrate  
 126 concentrations under different anthropogenic NO<sub>x</sub> emission reductions, respectively.  
 127 The bars (right y-axis) in panel (a) show the corresponding nitrate contribution from  
 128 soil Nr emissions (denoted as soil nitrate concentrations) under different anthropogenic  
 129 NO<sub>x</sub> emission reductions, which are determined as the difference between the solid and  
 130 dotted lines. The bars (right y-axis) in panel (b) show the suppression of nitrate  
 131 reduction due to the existence of soil nitrogen emissions (denoted as soil suppression),  
 132 which are determined as the difference between the solid and dotted lines. Green lines  
 133 and bars are the results in the FWP region, and the yellow are the results in the BTH  
 134 region.)

135



136 **Reference**

- 137 Finlayson-Pitts, B. J., Wingen, L. M., Sumner, A. L., Syomin, D., and Ramazan, K. A.:  
138 The heterogeneous hydrolysis of NO<sub>2</sub> in laboratory systems and in outdoor and  
139 indoor atmospheres: An integrated mechanism, *Phys. Chem. Chem. Phys.*, 5, 223-  
140 242, 10.1039/b208564j, 2003.
- 141 Fu, X., Wang, T., Zhang, L., Li, Q., Wang, Z., Xia, M., Yun, H., Wang, W., Yu, C., Yue,  
142 D., Zhou, Y., Zheng, J., and Han, R.: The significant contribution of HONO to  
143 secondary pollutants during a severe winter pollution event in southern China,  
144 *Atmos. Chem. Phys.*, 19, 1-14, 10.5194/acp-19-1-2019, 2019.
- 145 Li, G., Lei, W., Zavala, M., Volkamer, R., Dusanter, S., Stevens, P., and Molina, L. T.:  
146 Impacts of HONO sources on the photochemistry in Mexico City during the  
147 MCMA-2006/MILAGO Campaign, *Atmos. Chem. Phys.*, 10, 6551-6567,  
148 10.5194/acp-10-6551-2010, 2010.
- 149 Meng, F., Qin, M., Fang, W., Duan, J., Tang, K., Zhang, H., Shao, D., Liao, Z., Feng,  
150 Y., Huang, Y., Ni, T., Xie, P., Liu, J., and Liu, W.: Measurement of HONO flux  
151 using the aerodynamic gradient method over an agricultural field in the Huaihe  
152 River Basin, China, *J. Environ. Sci.*, 114, 297-307, 10.1016/j.jes.2021.09.005,  
153 2022.
- 154 Oswald, R., Behrendt, T., Ermel, M., Wu, D., Su, H., Cheng, Y., Breuninger, C.,  
155 Moravek, A., Mougín, E., Delon, C., Loubet, B., Pommerening-Röser, A., Sörgel,  
156 M., Pöschl, U., Hoffmann, T., Andreae, M. O., Meixner, F. X., and Trebs, I.:  
157 HONO Emissions from Soil Bacteria as a Major Source of Atmospheric Reactive  
158 Nitrogen, *Science*, 341, 1233-1235, 10.1126/science.1242266, 2013.
- 159 Rappenglück, B., Lubertino, G., Alvarez, S., Golovko, J., Czader, B., and Ackermann,  
160 L.: Radical precursors and related species from traffic as observed and modeled at  
161 an urban highway junction, *J. Air Waste Manage. Assoc.*, 63, 1270-1286, 2013.
- 162 Saliba, N. A., Mochida, M., and Finlayson-Pitts, B. J.: Laboratory studies of sources of  
163 HONO in polluted urban atmospheres, *Geophys. Res. Lett.*, 27, 3229-3232,  
164 10.1029/2000gl011724, 2000.
- 165 Sarwar, G., Roselle, S. J., Mathur, R., Appel, W., Dennis, R. L., and Vogel, B.: A

166 comparison of CMAQ HONO predictions with observations from the Northeast  
167 Oxidant and Particle Study, *Atmos. Environ.*, 42, 5760-5770,  
168 10.1016/j.atmosenv.2007.12.065, 2008.

169 Tang, K., Qin, M., Fang, W., Duan, J., Meng, F., Ye, K., Zhang, H., Xie, P., Liu, J., Liu,  
170 W., Feng, Y., Huang, Y., and Ni, T.: An automated dynamic chamber system for  
171 exchange flux measurement of reactive nitrogen oxides (HONO and NO<sub>x</sub>) in  
172 farmland ecosystems of the Huaihe River Basin, China, *Sci. Total Environ.*, 745,  
173 140867, 10.1016/j.scitotenv.2020.140867, 2020.

174 Twigg, M. M., House, E., Thomas, R., Whitehead, J., Phillips, G. J., Famulari, D.,  
175 Fowler, D., Gallagher, M. W., Cape, J. N., Sutton, M. A., and Nemitz, E.:  
176 Surface/atmosphere exchange and chemical interactions of reactive nitrogen  
177 compounds above a manured grassland, *Agric. For. Meteorol.*, 151, 1488-1503,  
178 10.1016/j.agrformet.2011.06.005, 2011.

179 Wang, Y., Fu, X., Wang, T., Ma, J., Gao, H., Wang, X., and Pu, W.: Large Contribution  
180 of Nitrous Acid to Soil-Emitted Reactive Oxidized Nitrogen and Its Effect on Air  
181 Quality, *Environ. Sci. Technol.*, 57, 3516-3526, 10.1021/acs.est.2c07793, 2023.

182 Weber B, W. D., Tamm A, et al. : Biological soil crusts accelerate the nitrogen cycle  
183 through large NO and HONO emissions in drylands, *Proc. Natl. Acad. Sci. U.S.A.*,  
184 112(50): 15384-15389., 2015.

185 Wu, D., Horn, M. A., Behrendt, T., Müller, S., Li, J., Cole, J. A., Xie, B., Ju, X., Li, G.,  
186 Ermel, M., Oswald, R., Fröhlich-Nowoisky, J., Hoor, P., Hu, C., Liu, M., Andreae,  
187 M. O., Pöschl, U., Cheng, Y., Su, H., Trebs, I., Weber, B., and Sörgel, M.: Soil  
188 HONO emissions at high moisture content are driven by microbial nitrate  
189 reduction to nitrite: tackling the HONO puzzle, *ISME J.*, 13, 1688-1699,  
190 10.1038/s41396-019-0379-y, 2019.

191 Wu, D., Zhang, J., Wang, M., An, J., Wang, R., Haider, H., Xu-Ri, Huang, Y., Zhang,  
192 Q., Zhou, F., Tian, H., Zhang, X., Deng, L., Pan, Y., Chen, X., Yu, Y., Hu, C., Wang,  
193 R., Song, Y., Gao, Z., Wang, Y., Hou, L., and Liu, M.: Global and Regional Patterns  
194 of Soil Nitrous Acid Emissions and Their Acceleration of Rural Photochemical  
195 Reactions, *J. Geophys. Res.: Atmos.*, 127, 10.1029/2021jd036379, 2022.

196 Xue, C., Ye, C., Zhang, Y., Ma, Z., Liu, P., Zhang, C., Zhao, X., Liu, J., and Mu, Y.:  
197 Development and application of a twin open-top chambers method to measure soil  
198 HONO emission in the North China Plain, *Sci. Total Environ.*, 659, 621-631,  
199 10.1016/j.scitotenv.2018.12.245, 2019.

200 Zhang, J., An, J., Qu, Y., Liu, X., and Chen, Y.: Impacts of potential HONO sources on  
201 the concentrations of oxidants and secondary organic aerosols in the Beijing-  
202 Tianjin-Hebei region of China, *Sci. Total Environ.*, 647, 836-852,  
203 10.1016/j.scitotenv.2018.08.030, 2019.

204 Zhang, L., Wang, T., Zhang, Q., Zheng, J., Xu, Z., and Lv, M.: Potential sources of  
205 nitrous acid (HONO) and their impacts on ozone: A WRF-Chem study in a  
206 polluted subtropical region, *J. Geophys. Res.: Atmos.*, 121, 3645-3662,  
207 10.1002/2015jd024468, 2016.

208 Zhou, X., Zhang, N., TerAvest, M., Tang, D., Hou, J., Bertman, S., Alaghmand, M.,  
209 Shepson, P. B., Carroll, M. A., Griffith, S., Dusanter, S., and Stevens, P. S.: Nitric  
210 acid photolysis on forest canopy surface as a source for tropospheric nitrous acid,  
211 *Nat. Geosci.*, 4, 440-443, 10.1038/ngeo1164, 2011.

212